# Modeling of Impact-Driven Shock-to-Detonation Transition in Porous PBX 9502

Joshua D. Garno, Mark Short, Stephen J. Voelkel, Carlos Chiquete
Shock and Detonation Physics Group, Los Alamos National Laboratory
Los Alamos, NM, USA

## 1 Introduction

Solid high explosives (HEs) consist of energetic crystals of various particle sizes and properties [1]. Additionally, polymer-bonded explosives (or PBXs), such as the HMX-crystal based PBX 9501 or TATB-crystal based PBX 9502, combine the explosive crystal with polymers to create a molding powder which, after pressing, results in a cohesive HE material [2, 3]. While the pressing process is typically conducted under high pressures and temperatures, the resistance to compaction due to the structural irregularity of the powder results in some residual porosity in the HE [4]. For instance, PBX 9502 is pressed to within a target density range of $1.890 \pm 0.005$ g/cm$^3$. With a theoretical maximum density (TMD) of $1.941$ g/cm$^3$ [2], the solid volume fraction is $0.97-0.98$. Significant additional porosity can also be introduced into a PBX through thermal or mechanical damage. Porosity has long been recognized as an integral component in the shock initiation behavior of HEs, with pore collapse potentially contributing to the formation of hot-spots [5]. For the case of highly porous HEs like PETN, it has also been shown that increasing porosity results reduces the stress input required to achieve detonation within a certain length [4].

The driving physical processes through which porosity contributes to the detonation initiation process are yet to be described or modeled in detail. The purpose of this study is to model the mechanisms by which additional porosity, resulting in initial densities lower than the target pressing density, could affect the shock initiation behavior of the insensitive HE PBX 9502. We consider a one-dimensional configuration in which a Kel-F 81 flyer impacts PBX 9502 at some prescribed velocity $V_{im}$ (Fig.1). A new, material-symmetric, compressible, continuum-level mixture modeling framework is employed. The HE material component within the mixture model is PBX 9502 pressed to a target density range of $1.890 \pm 0.005$ g/cm$^3$. The shock initiation behavior of this PBX 9502 mixture component is modeled with a recalibrated Wescott-Stewart-Davis (WSD), pressure-dependent, reactive burn model [6]. With no additional porosity, we assume this PBX 9502 material to have a volume fraction of one within the mixture model framework. Additional porosity is then added into the PBX 9502 through the introduction of a void component in the mixture model, reducing the initial volume fraction of PBX 9502.

In order to gain some insights into the competing physics with regard to initiation effects, consider a shock wave running into non-porous versus porous PBX 9502. For a fixed shock speed, the pressure generated in the porous material at equilibrium assuming no reaction will generally be higher than that generated in the non-porous material due to the effects of compaction [7]. With a pressure-dependent

Correspondence to: jgarno@lanl.gov 

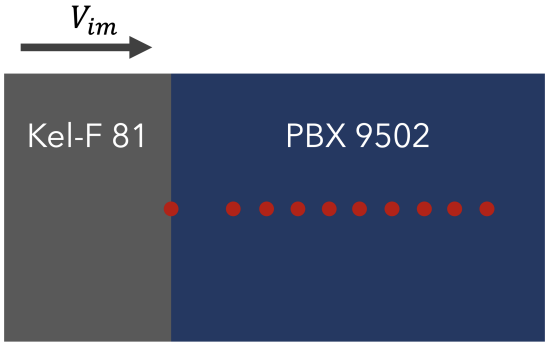


Figure 1: Schematic diagram of a Kel-F 81 projectile impacting a PBX 9502 target. The red dots indicate the presence of embedded particle velocity gauges in the PBX 9502.

reaction rate such as for the WSD model, this would result in a faster initiation time, or equivalently a shorter run-to-detonation distance, in the porous material. However, for the Kel-F 81 impactor configuration, the strength of the shock entering the PBX 9502 will become progressively weaker for increasingly porous PBX 9502 for a fixed impact speed. Thus, determining the relative run-to-detonation distances for detonation initiation becomes a competition between the lower input shock strength for increasingly porous PBX 9502, and the relative increase in pressure that results from the compaction process behind the shock. In order to address these effects, we present a series of hydrodynamic simulations, parameterized by Kel-F flyer impact velocity, initial HE porosity, and compaction length scale. Primary prediction metrics include time to initiation, run-to-detonation distance, and detonation speed.

## 2 Modeling

Our flow configuration is shown in Fig. 1. The moment of Kel-F projectile contact with the PBX 9502 target serves as the initial condition for the simulations. The governing equations for each material (Kel-F and PBX 9502) are given by

$$\frac{\partial(\alpha_i)}{\partial t} + u\frac{\partial(\alpha_i)}{\partial x} = \mathcal{F}_i = \sum_{j,j\neq i}\left[\mathcal{F}_{ij}\right] + \mathcal{F}_{iv}\,, \quad \frac{\partial(\alpha\rho)_i}{\partial t} + \frac{\partial(\alpha\rho u)_i}{\partial x} = 0\,, \tag{1}$$

$$\frac{\partial(\alpha\rho u)_i}{\partial t} + \frac{\partial(\alpha[\rho u^2+p])_i}{\partial x} = m_i^+\,, \quad \frac{\partial(\alpha\rho E)_i}{\partial t} + \frac{\partial}{\partial x}\left(\alpha\rho u\left[E+\frac{p}{\rho}\right]\right)_i = e_i^+\,, \tag{2}$$

where $\{\alpha, \rho, u, p, E\}_i$ are the volume fraction, density, velocity, pressure, and total specific energy ($E_i = e_i + u_i^2/2$, where $e_i$ is the specific internal energy) of material $i$, where $i = 1$ (Kel-F 81 projectile), or 2 (PBX 9502 target). Generally, coexistent materials exchange momentum and energy via source terms $m_i^+$ and $e_i^+$, respectively, while the compaction rate of each material is given by $\mathcal{F}_i$. Conservation of momentum and energy in the system dictates that $m_1^+ = -m_2^+$ and $e_1^+ = -e_2^+$, respectively. Volume saturation is enforced by material-pair compaction rates obeying $\mathcal{F}_{ij} = -\mathcal{F}_{ji}$ and $\alpha_v = 1 - \sum_j \alpha_j$, where $\alpha_v$ is the local volume fraction of voids (or porosity). Material porosity is accounted for by material-void compaction rates $\mathcal{F}_{iv}$. The inert Kel-F 81 projectile is modeled with a Mie-Gruneisen equation of state (EOS) of the form $e_i = e_i(\rho_i, p_i)$, where $i = 1$ and $\rho_0 = 2.14$ g/cc, $c = 2.05$ mm/$\mu$s, $\Gamma_0 = 1.5$, and $s = 1.65$ for the linear Us-Up reference curve (see [2, 7] for details regarding standard parameter definitions). The reactant and product EOSs of form $e_i = e_i(\lambda_i, \rho_i, p_i)$ for $i = 2$ and reaction rate for the PBX 9502 target are given by a recalibrated form of the WSD model of [6] using $p - \rho$ closure [8], with the evolution of reaction progress, $\lambda_2$, given by

$$\frac{\partial(\alpha\rho\lambda)_2}{\partial t} + \frac{\partial(\alpha\rho\lambda u)_2}{\partial x} = \alpha_2\rho_2\Lambda_2, \tag{3}$$

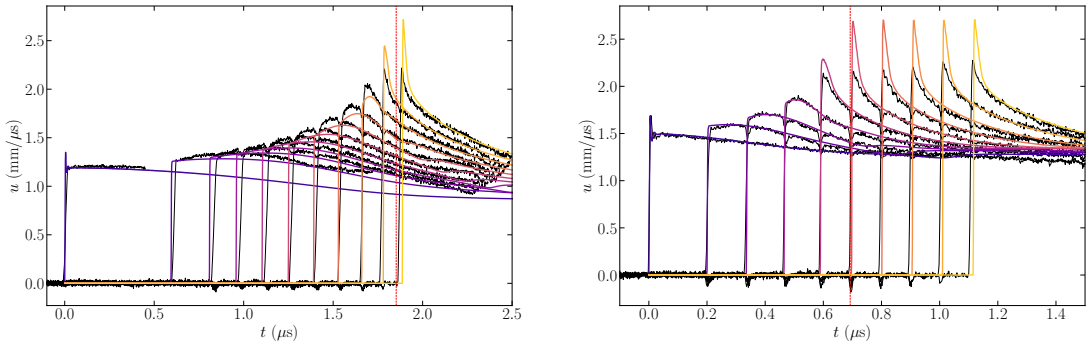


Figure 2: Comparison of embedded gauge particle velocity traces between experiments and simulations for $V_{im} = 2.493$ mm/$\mu$s (Left) and $V_{im} = 3.118$ mm/$\mu$s (Right). The black lines are experimental measurements, while the colored lines are simulation results at the corresponding gauge locations.

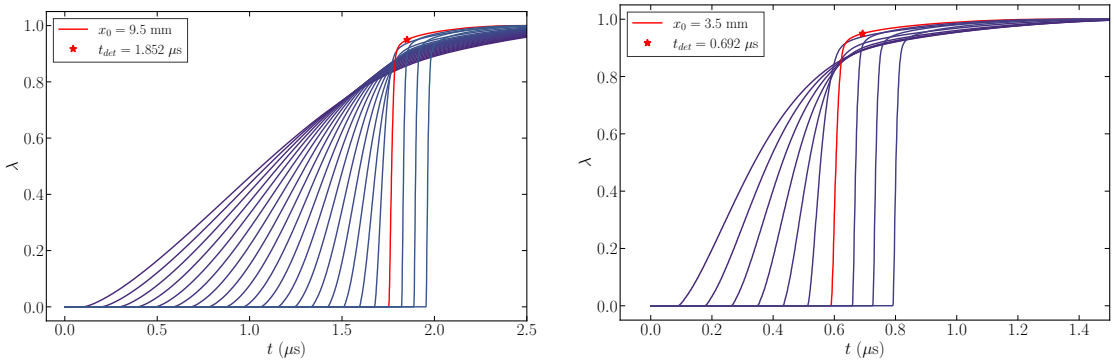


Figure 3: Simulations of the evolution of reaction progress, $\lambda$, with time along various embedded particle velocity gauges for $V_{im} = 2.493$ (Left) and $V_{im} = 3.118$ mm/$\mu$s (Right). Here, $x_0$ indicates the initial depth of the gauge in which detonation was first reached, with adjacent gauges 0.5 mm apart. Time to detonation, $t_{det}$, for each shot was determined as the minimum time over all gauges to reach $\lambda = 0.95$.

where $\lambda_2 \in [0, 1]$, and $\Lambda_2$ is the reaction rate. Standard finite volume methods are used to integrate the system on a one-dimensional, uniform, structured mesh. Spatial discretization is performed using a second order Lax-Friedrichs flux with minmod reconstruction, and temporal integration by a second order TVD Runge-Kutta method. A cell spacing of 5 $\mu$m was found to be provide mesh converged resolution of the compaction and reaction layers for the purposes of this study.

## 3 Results

We have recalibrated the WSD reactive burn on the detonation initiation branch for nominal density PBX 9502 using embedded (particle velocity) gauge data from four experimental tests at different impact speeds [2]. Figure 2 shows the experimental particle velocity traces from embedded gauges corresponding to Kel-F flyer impact velocities of $V_{im} = 2.493$ mm/$\mu$s and $V_{im} = 3.118$ mm/$\mu$s. Also shown is the corresponding calibrated simulation data. The calibration is able to successfully reproduce the timing of wave arrival at each gauge, build-up of reaction, and transition to detonation. The prediction of time-to-detonation, $t_{det}$, was determined as the minimum time for any embedded gauge to first reach $\lambda = 0.95$ (Fig. 3). The corresponding run-to-detonation, $x_{det}$, i.e. the distance traversed by the shock between the times of impact and detonation, was found by linear interpolation of the shock trajectory to $t = t_{det}$.

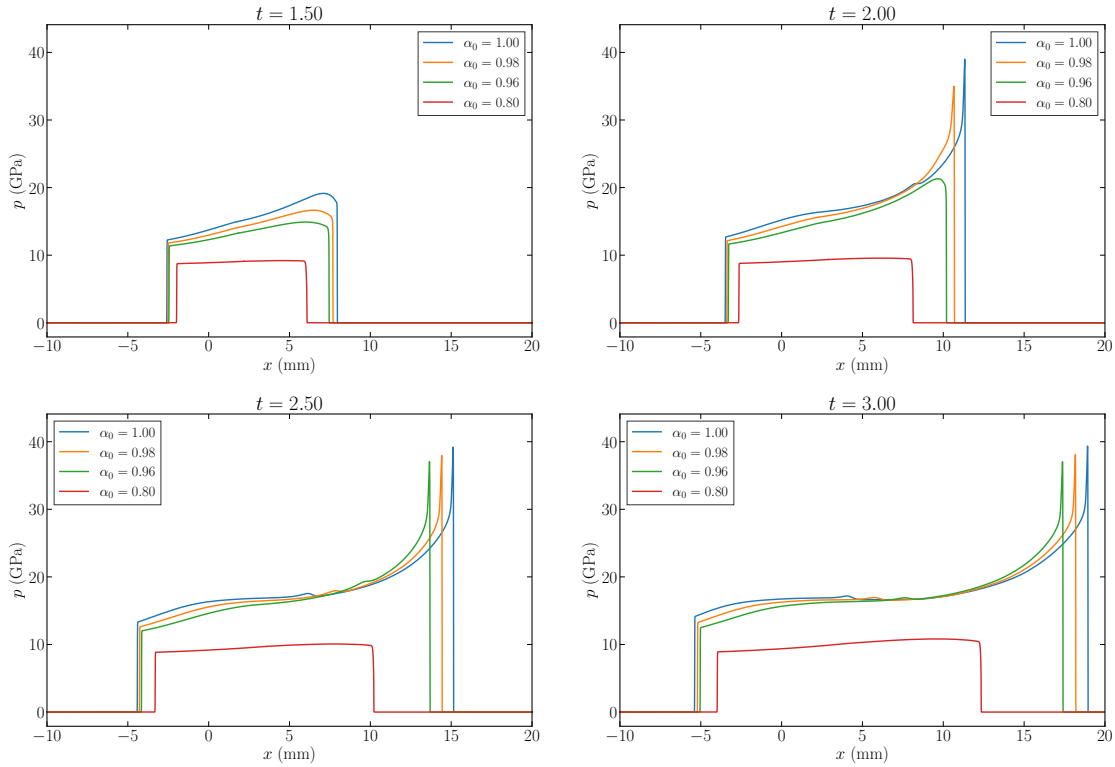


Figure 4: Mixture pressure, $p = \sum_i \alpha_i p_i$, for a given initial HE porosity ($\alpha_0$) at four time instances (given in $\mu$s) for $V_{im} = 2.493$ mm/$\mu$s. At $t = 0$, $x < 0$ contains Kel-F 81, and $x > 0$ contains PBX 9502. The PBX 9502 compaction viscosity is $\mu_{2v} = 0.1$ GPa·$\mu$s.

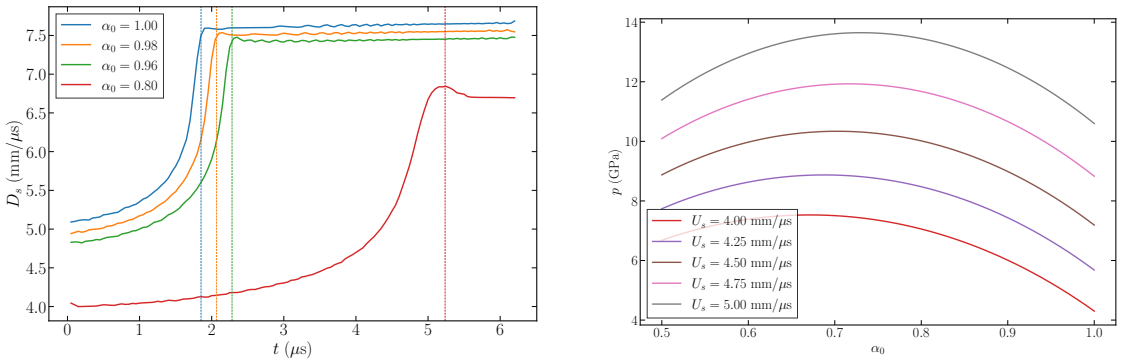


Figure 5: (Left) Shock speed evolution corresponding to Fig. 4 for the given $\alpha_0$. The dotted lines show $t_{det}$ for each case. (Right) Compaction equilibrium pressure in PBX 9502 (without reaction) as a function of $\alpha_0$ for the three fixed wave speeds shown.

With the recalibrated WSD model for nominal density PBX 9502, we conduct a series of computational predictions on the effect of additional PBX 9502 porosity on the detonation initiation process. Figure 4 shows the evolution of the mixture pressure, $p = \sum_i \alpha_i p_i$, for a Kel-F impact speed of $V_{im} = 2.493$ mm/$\mu$s and for initial HE porosities of $\alpha_0 = 1$, 0.98, 0.96 and 0.8, corresponding to initial PBX 9502 densities of $\rho_0 = 1.895$, 1.857, 1.820, 1.526 g/cm$^3$ (as noted above, we assume that $\alpha_0 = 1$ for the nominal density PBX 9502). The PBX 9502 compaction viscosity $\mu_{v2}$ that appears in $F_{2v}$ (1) was 0.1 GPa·$\mu$s, so that compaction should occur significantly more rapidly than reaction. For the porous PBX

Table 1: Prediction of the run-to-detonation time and location for $V_{im} = 2.493$ mm/$\mu$s for varying $\alpha_0$ and $\mu$.

| Shot | $\alpha_0$ | $\rho_0$ (g/cc) | $p_{eq}$ / $p_{sh}$ (GPa) | $\mu$ (GPa $\cdot\mu$s) | $t_{det}$ ($\mu$s) | $x_{det}$ (mm) |
|---|---|---|---|---|---|---|
| 2S-69 | 1.00 | 1.895 | 11.62 | - | 1.852 | 10.234 |
| | 0.98 | 1.857 | 11.30 / 10.60 | 4.00 | 2.316 | 13.026 |
| | | | | 2.00 | 2.311 | 12.896 |
| | | | | 0.10 | 2.068 | 11.194 |
| | 0.96 | 1.820 | 10.99 / 9.68 | 4.00 | 2.564 | 14.143 |
| | | | | 2.00 | 2.553 | 13.907 |
| | | | | 0.10 | 2.282 | 12.069 |
| | 0.80 | 1.516 | 8.78 / 4.79 | 4.00 | 5.962 | 28.964 |
| | | | | 2.00 | 5.282 | 24.092 |
| | | | | 0.10 | 5.237 | 23.833 |

9502, even with the increase in pressure generated due to this rapid compaction, the pressures observed in the porous PBX 9502 shortly after impact are less than those found in the nominal density material. As a result, pressure build-up due to reaction occurs most rapidly in the nominal density material, with pressure building up progressively more slowly as the porosity increases. Both the time to detonation and run-to-detonation length increase as $\alpha_0$ decreases, as seen in Fig. 4. A summary of $t_{det}$ and $x_{det}$ for each $\alpha_0$ is given in Table 1. Note that pressure build-up due to reaction occurs near the lead front in all additional porosity cases. Figure 5 shows the corresponding shock speed evolution for the given $\alpha_0$. Relative shock speeds and accelerations are lower as the porosity increases.

As noted in §1, as the PBX 9502 porosity increases, for a fixed Kel-F flyer impact speed $V_{im}$, the strength of the lead shock that is transmitted into the PBX 9502 decreases. For rapid compaction relative to the rate of reaction, the equilibrium pressure obtained after compaction of the porous material can be significantly larger than that behind the lead shock wave. In fact, for any fixed shock speed in the PBX 9502, the equilibrium pressure due to compaction first increases as the porosity increases (Fig. 5 (Right)). The question then becomes whether or not the decrease in shock pressure due to the decrease in lead shock strength for decreasing $\alpha_0$ at fixed $V_{im}$ can be overcome by the effects of compaction, so that the compaction equilibrium pressure is above that attained at the shock front in the nominal density PBX 9502. Figure 6 (Left) shows that this is not the case for the three additional porosity cases studied in Fig. 4 across a wide range of impact speeds $V_{im}$. Figure 6 (Right) shows that this would also generally be the case for any $\alpha_0$ considered. Finally, Fig. 7 and table 1 shows that increasing the compaction viscosity leads to longer detonation initiation times, as expected.

In summary, for the shock initiation problem of a flyer impacting PBX 9502, we find that increasing porosity will result in an increase in run-to-detonation time and length under the model described in §2. It is possible to reverse this behavior by making changes to the model, such as making the reaction rate a function of porosity [9]. We also note that within this modeling framework, it is possible to explore several other flow configurations. For instance, we will additionally consider the onset of detonation due to hot-spot initial conditions. Here, the porosity can support the development of subsonic compaction waves in the PBX 9502 which can generate significant pressures, whereas the non-porous material cannot.

## References

[1] C.A. Handley, B.D. Lambourn, N.J. Whitworth, H.R. James, and W.J. Belfield. Understanding the shock and detonation response of high explosives at the continuum and meso scales. *Appl. Phys. Rev.*, 5:011303, 2018.

[2] R.L. Gustavsen, S.A. Sheffield, and R.R. Alcon. Measurements of shock initiation in the tri-amino-

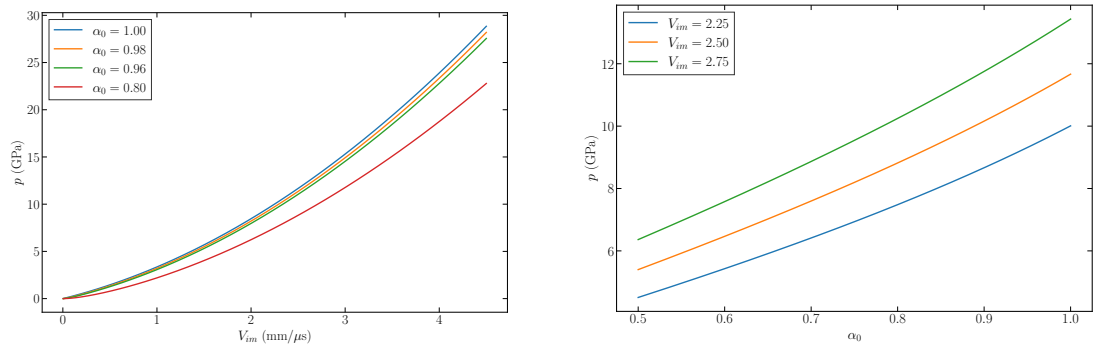


Figure 6: (Left) The compacted-state equilibrium pressure in the PBX 9502 as a function of flyer speed $V_{im}$ for the $\alpha_0$ shown, assuming no reaction. (Right) Compacted equilibrium pressure in PBX 9502 (without reaction) as a function of $\alpha_0$ for the three $V_{im}$ speeds shown.

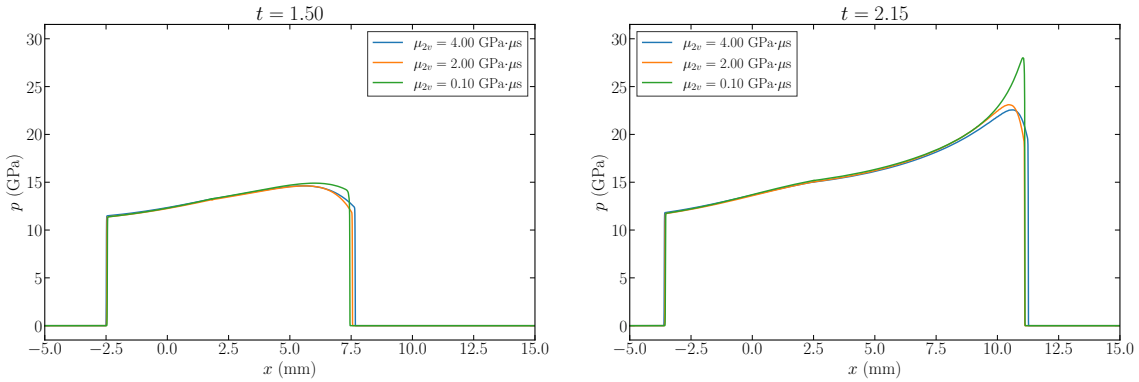


Figure 7: Mixture pressure, $p = \sum_i \alpha_i p_i$, for various $\mu_{2v}$ for $\alpha_0 = 0.96$ and $V_{im} = 2.493$ mm/$\mu$s at two time instances (given in $\mu$s).

tri-nitro-benzene based explosive PBX 9502: Wave forms from embedded gauges and comparison of four different material lots. *J. Appl. Phys.*, 99(11):114907, 2006.

[3] S.J. Voelkel, E.K. Anderson, M. Short, C. Chiquete, and S.I. Jackson. Effect of lot microstructure variations on detonation performance of the triaminotrinitrobenzene (TATB)-based insensitive high explosive PBX 9502. *Combust. Flame*, 246:112373, 2022.

[4] S.A. Sheffield, R.L. Gustavsen, and M.U. Anderson. Shock loading of porous high explosives. In *High-Pressure Shock Compression of Solids IV*, pages 23–61. Springer, 1997.

[5] E.L. Lee and C.M. Tarver. Phenomenological model of shock initiation in heterogeneous explosives. *Phys. Fluids*, 23(12):2362–2372, 1980.

[6] B.L. Wescott, D.S. Stewart, and W.C. Davis. Equation of state and reaction rate for condensed-phase explosives. *J. Appl. Phys.*, 98(5):053514, 2005.

[7] M. Short and J.J. Quirk. The effect of compaction of a porous material confiner on detonation propagation. *J. Fluid Mech.*, 834:434–463, 2018.

[8] M. Short, C. Chiquete, J.B. Bdzil, and J.J. Quirk. Detonation diffraction in a circular arc geometry of the insensitive high explosive PBX 9502. *Combust. Flame*, 196:129–143, 2018.

[9] J.A. Sáenz and D.S. Stewart. Modeling deflagration-to-detonation transition in granular explosive pentaerythritol tetranitrate. *J. Appl. Phys.*, 104:043519, 2008.